The Effect of Microstructure on Fatigue Properties of High Density Ferrous P/M Materials

Howard Rutz, Thomas Murphy and Tina Cimino
Hoeganaes Corporation
Riverton, NJ U.S.A.

ABSTRACT

Fatigue testing (rotating bending fatigue) has been performed on several high performance ferrous P/M material systems. Detailed metallographic analysis was performed to determine differences in the failure mechanisms for various material and process combinations. A variety of material compositions were single compacted to high density via the ANCORDENSE^{TM} compaction system. This was followed by conventional and high temperature sintering and testing in the as-sintered and heat treated conditions. The analysis provides information as to the relationships between density, structure and composition with fatigue life.

INTRODUCTION

The application of ferrous powder metallurgy components in more demanding applications requires a better understanding of the effect of material selection and processing techniques on optimizing fatigue properties. In the current study, fatigue properties have been evaluated utilizing the rotating bending fatigue (RBF) method for a wide variety of material compositions and processing routes. In addition, the materials involved in the study were evaluated to determine tensile properties for a comparison with the fatigue properties. A metallographic evaluation was performed to determine which microstructural constituents were present in the tested materials. Stereological studies were performed to evaluate the effect of pore size, shape and morphology on fatigue performance.

MATERIALS AND PROCESSING

Several material compositions were selected for the study and appropriate binder treated premixes were prepared. The compositions are listed in Table I.

The materials were compacted into test specimens utilizing the ANCORDENSE[3] warm compaction system. Compaction was performed at 290°F/140°C at a variety of compaction pressures to obtain a range of density levels. Table II lists the sintering and heat treatment schedules followed for the study along with the density levels for each material. Sintering was performed at the stated temperature in a 75v/o HJ25v/o N_2 atmosphere for 30 minutes at temperature. Following sintering, material B was tempered at 375°F/190°C for one hour in air before being tested in the as sintered state. Heat treatment of selected specimens, was performed as follows:

Austenitize:	One hour at 1650°F/900°C
Atmosphere:	Endothermic with a slightly positive carbon potential
Quench:	Oil at 165°F/75°C
Temper:	One hour at 375°F/190°C in air

The as-sintered fatigue samples were machined and ground to size following the sintering operation. The heat treated tensile and fatigue samples were rough machined following sintering then heat treated, finish ground, and lastly polished to size.

TESTING PROCEDURES AND RESULTS

Following sample preparation, density was determined on representative samples using the immersion technique outlined in MPIF Standard 423. The tensile properties were ascertained for the as-sintered materials on dogbone tensile specimens according to MPIF Standard 104. Heat treated tensile properties were determined from machined threaded specimens. In most cases, the density involved in tensile testing did not exactly match the density of the fatigue specimens. When this was the case, the tensile properties reported were extrapolated from the available data to insure that the two sets of data were as comparable as possible.

As mentioned above, the rotating bending fatigue specimens were machined following sintering either to final size for the as-sintered materials, or rough machined prior to heat treatment and ground to size following heat treatment. The dimensions of the fatigue specimen are shown in Figure 1. Fatigue testing was performed on six Fatigue Dynamics RBF-200 machines utilizing a speed of 8000 rpm. The six machines were selected randomly for each material test. A run out test was established to be at 10 million cycles. Testing was performed on between 20 to 30 specimens per material to establish the fatigue endurance limit (FEL) of the materials. The initial portion of the test utilized a staircase method to define two stress levels. These target levels provided one level where about half of the samples failed and the second where significantly less than half of the specimens failed. Based on these results, a two point estimate of 50% (50% FEL) and 0.1% (99.9% FEL) failure rates were established by linear extrapolation of the data plotted on a normal probability chart. Tables III through V list the results of RBF and tensile tests.

In addition to tensile and fatigue testing, failed fatigue specimens underwent metallographic examination. The etched microstructures were analyzed to determine the microstructural constituents present and the results are presented in Tables VI through VIII. The pore structures of the samples were quantified utilizing a Leitz TAS+ automated image analysis system according to established techniques illustrated by DeHoff and Aigeltinger[5]. Stereological techniques were used to determine, among others, mean pore size, number of pores per area and mean pore spacing (edge to edge). The stereological results for the materials are listed in Tables IX through XI.

DISCUSSION

In order to evaluate their effects on fatigue performance, individual properties were plotted versus the 50% FEL. The 50% FEL was selected because it provides an appropriate comparison of data between materials while limiting the potential extrapolation error that might be associated with 99.9% FEL data. The following section will compare the effect of density, ultimate tensile strength, microstructure, and mean pore spacing with fatigue properties of the various materials and processing techniques. The analysis was performed by sorting the materials into three processing groups; 2050°F/1120°C as-sintered, 2300°F/1260°C as-sintered and 2050°F/2350°F (1120°C/1290°C) heat treated. In this manner, materials processed in a similar fashion can be compared easily. Where possible, the scaling for the plots was kept

consistent so that an analysis of effects could be performed easily.

Sintered Density

The effect of sintered density on 50% FEL is shown in Figures 2 through 4. In all cases where a material was tested at two density levels, the data indicate that the 50% FEL increased with increasing density. The amount of improvement appeared to be a function of both the sintering temperature and the material composition. Material E indicates the lowest improvement with density in all three material groups. On average, material E improved at a rate of 1,300 psi
(9 MPa) for each increase in density of 0.1 g/cm^3. The rate of increase for material E was very consistent (1,400, 1,300, 1,400 psi per 0.1 $g/cm^{3)}$ regardless of the processing technique.

For the other materials, the amount of improvement in the 50% FEL as the density is increased appears to be more significant with the higher sintering temperature. In the case of the as-sintered materials, at 2300°F/1260°C, the average increase is about 4,000 psi (28 MPa) per 0.1 g/cm^3 while at 2050°F/1120°C the increase averages only 1,900 psi (13 MPa) per 0.1 g/cm^3. In the case of the heat treated data, only one high temperature sintered material was evaluated but it shows a high rate of change also (5,500 psi (38 MPa) per 0.1 $g/cm^{3)}$ versus the two Low temperature sintered materials. The rates of change for the two Low temperature materials are in line with what was observed with the as-sintered results.

The analysis provided only two data points for each material and the amount of variation in density is relatively small (about 0.2 g/cm3). Additional studies will be required to evaluate the effect of density fully. Additionally, although the amount of improvement found with density for a given material appears to be substantial, the differences between materials appear to be more dominant in determining the fatigue properties.

Ultimate Tensile Strength

Figures 5 through 7 indicate the relationship between ultimate tensile strength and 50% FEL. The improvement in strength realized by higher density for a given material is indicated as an increase in 50% FEL. As with density, there appears to be no direct relationship between ultimate tensile strength and fatigue properties when comparing several materials processed in a similar manner. As an example, material A sintered at either 2050°F/1120°C or 2300°F/1260°C results in the lowest value for ultimate tensile strength of the materials examined while material E results in the highest values. Material A sintered at 2050°F/1120°C at a density of 7.40 g/cm^3 has a tensile strength of 59,000 psi (403 MPa) and a 50% FEL of 32,700 psi (225 MPa). Material E processed in a similar fashion to a density of 7.19 g/cm^3 obtained an ultimate tensile strength of 103,000 psi (710 MPa) or nearly twice that of material A. However, in this condition, material E showed a 50% FEL value of only 33,000 psi (228 MPa), nearly the same as material A despite the much higher ultimate tensile strength. Material A's 50% FEL was about 56% of the ultimate strength while material E's 50% FEL was only about 30% of the ultimate strength.

For a given material, the microstructure resulting from a processing route (i.e. as-sintered versus heat treated) appeared to have the most important effect on fatigue properties. Material B obtained an as-sintered ultimate strength of 133,000 psi (917 MPa) at a density of 7.27 g/cm^3 and a heat treated ultimate strength of 196,000 psi (1350 MPa) at the same density or an increase of 47%. The 50% FEL, however, was increased by 66% from 39,200 psi (270 MPa) to 65,100 psi (449 MPa). This information indicates that the density and microstructure developed by varying the processing techniques may be more indicative of the resulting fatigue properties than the utilization of ultimate strength results.

Microstructure

In this section, an analysis was completed to evaluate whether the presence of particular microstructural components (ferrite, pearlite, martensite, etc.) was critical in defining fatigue properties. The role of pores and pore structure will be discussed in the stereological discussion.

Each of the material processing combinations was examined in the area of fracture to determine the type of microstructural constituents present and evaluate if the fracture path could be related to a particular microstructural feature. It is unclear whether this analysis technique would reveal any important information relative to the fatigue performance as this method analyzes where the crack propagated rather than how the crack initiation occurred. In materials where crack initiation is critical, it would be nearly impossible to evaluate the material utilizing these techniques. Detailed fracture toughness effects would be more appropriate.

In reviewing the as-sintered materials, it would appear that the presence of an all ferrite microstructure in material A resulted in highest ratio of 50% FEL to ultimate strength. No other direct relationships between microstructural constituents and fatigue properties were found. The same statement could be made concerning the heat treated materials, where the microstructures were predominantly various forms of martensite, it should be noted that the heat treated materials did obtain higher 50% FEL values than the as-sintered materials.

For all materials, crack propagation appeared not to be related to the presence of any one microstructural component but rather to the presence of pores. One possible exception was found in the heat treated sample of material B. The microstructure of this material consisted of light and dark etching martensite. It is likely that the light etching areas contained higher alloy content; in particular, higher amounts of nickel and chromium. The cracks in this material appeared to avoid the dark etching areas in preference to the light etching areas (Figure 8). It should be noted that the cracks in this material also appeared to be related to the pore structure and that there appeared to be a higher preponderance of pores in the light etching areas. It is impossible therefore to judge whether the light etching structure itself is lower in fatigue strength or whether the pores present in this area contributed to the lower strength.

An additional microstructural feature that appeared to influence fatigue properties was grain size. Four of the materials (A, E, H, and I) were tested in the as-sintered

state following sintering at both 2050°F/1120°C and 2300°F/1260°C. In alt four cases, the microstructural examination revealed that the higher sintering temperature resulted in a coarser grain structure. Materials E, H, and I also contained nickel additions. The materials sintered at the lower temperature all contain higher levels of nickel rich regions due to less complete diffusion of the nickel during sintering. Both the grain size and nickel diffusion effects are shown for Material I in Figure 9.

Figure 10 shows a comparison of fatigue properties for these four materials versus density. In the case of the three nickel bearing materials, the fatigue properties clearly were lowered with increasing sintering temperature indicating that either the finer grain size or the presence of nickel rich areas in the lower temperature sintered materials resulted in improved fatigue performance. It is more difficult to determine the effect of sintering temperature in the case of material A. The density and fatigue properties were increased significantly by raising the sintering temperature. Since the density levels studied are considerably different from each other and only two density levels were studied, the exact effect is somewhat unclear.

STEREOLOGICAL ANALYSIS

Several potential parameters were examined to determine if pore formation had a significant impact on fatigue properties. Figures 11 through 13 show the relationship between mean pore spacing and the 50% FEL for the materials grouped by processing technique. It is clear from these plots that in the case of as-sintered materials, the pore spacing appears to play an important role in fatigue performance. For a given material, the graphs indicate that as the pore spacing is increased due to increasing density, the fatigue properties are increased also. Interestingly, for a given processing condition, the pore spacing presents a reasonable prediction of 50% FEL. The one exception is material A which follows the same trend but differs from the other materials processed in a similar fashion. The fact that the microstructure of material A is considerably different than that of the other materials would appear to be a reasonable explanation of the difference.

In considering the materials D and H sintered at 2050°F/1120°C for example; the density, the number of pores and the mean pore size are quite different due to different premix alloy additions (copper and nickel). The evolution of porosity during sintering of these two materials produces very different pore structures. Premix additions of coarse copper result in fewer, but larger pores (material D) and additions of fine nickel results in more, but smaller pores (material H). Furthermore, density levels at the lower compacting pressure also show a large difference, 7.07 versus 7.18 g/cm^3 respectively. The lower density material (D) had fewer pores by comparison but the mean pore size was considerably larger. As a result of these differences, the mean pore spacing was nearly identical (61 versus 62 µm) and the 50% FEL values essentially were identical (33,000 psi/228 MPa). The combination of lower density and fewer, but larger pores resulted in the same pore spacing and performance as a the material with higher density and more, but smaller pores.

The data for the heat treated materials (Figure 13) is not as clear cut. The trends for each material are similar to the as-sintered results but a clear relationship between materials is not apparent. Interestingly, the stereological data for the materials tested

both in the as-sintered and heat treated conditions (materials B and E) are nearly identical. This indicates that the porosity of these two materials was not changed significantly during heat treatment.

It is clear that although the pore spacing appears to be a powerful tool for understanding fatigue properties, the values are not interchangeable between processes. Sintering at elevated temperatures will result in higher pore spacing due to a general reduction in the number of pores per area and an increase in pore size. However, as discussed above, the fatigue performance for the materials in this study was not enhanced with elevated sintering temperatures. Figure 14 shows the effect of pore spacing on 50% FEL as a function of sintering temperature. Despite increases in mean pore spacing with the higher sintering temperature, the fatigue values are lower. The correlation between mean pore spacing and 50% FEL remains for both conditions and the shape of the lines are similar.

CONCLUSIONS

- A number of P/M materials were evaluated to determine fatigue properties utilizing the rotating bending fatigue test. The influence of sintered density levels, ultimate tensile strength, microstructure and pore spacing on fatigue strength was examined. The following can be concluded from the studies:

- As the density of a particular material is increased, fatigue properties also increase. The amount of improvement in fatigue properties for a given increase in density was observed to be higher when sintering at elevated temperatures.

- A comparison of a wide variety of materials indicates that there is little correlation between ultimate tensile strength and fatigue properties. For a given material, as the density increases, so does the ultimate tensile strength and thus the fatigue properties.

- Material A, which is composed of ferrite, exhibited very high fatigue properties relative to Low ultimate tensile strength. Materials that were heat treated and were composed of very high amounts of tempered martensite gave the best fatigue properties.

- For materials that were sintered at two sintering temperatures, the lower sintering temperature resulted in higher fatigue performance for a given density. Two possible explanations have been presented. The higher temperature sintered materials exhibited a coarser grain structure than the same composition sintered at lower temperatures, which may have lowered the fatigue performance. The three materials that showed the most striking difference in fatigue properties also contained nickel. The Low temperature sintered materials contained a higher proportion of nickel rich areas while in the higher temperature sintered materials, the nickel was more uniformly diffused and resulted in a smaller amount of nickel rich areas.

- For materials processed in a similar manner, fatigue properties appear to be related closely to mean pore spacing. As the distance between pores is increased,

the fatigue properties are improved.

- The data presented in this paper indicate that predicting the fatigue properties of a P/M material involves a complex relationship between mean pore spacing, the grain size of the matrix material and the type and strength of the microstructural constituents present.

REFERENCES

1. Rutz, H.G., Luk, S.H., "Method of Making a Sintered Metal Component", United States Patent No. 5,154,881.

2. Luk, S.H., "Metal Powder Compositions Containing Binder Agents for Elevated Temperature Compaction", United States Patent No. 5,368,630-Additional Patents Pending.

3. Rutz, H.G., Hanejko, F.G., "High Density Processing of High Performance Ferrous Materials", *Advances in Powder Metallurgy & Particulate Materials- 1994,* Vol. 5, pp 117-133, Metal Powder Industries Federation, Princeton, NJ.

4. "Standard Test Methods for Metal Powders and Powder Metallurgy Products", Metal Powder Industries Federation, Princeton, NJ, 1993.

5. DeHoff, R.T., Aigeltinger, E.H., "Experimental Quantitative Microscopy With Special Applications to Sintering", Perspectives in Powder Metallurgy--Volume 5--Advanced Experimental Techniques in Powder Metallurgy, pp 81-137, Plenum Press, New York--London, 1970.

Table I: The Premix Compositions for the Materials in the Study

Material	Nominal Prealloy Content			Nominal Premix Additions					
	Mo (w/o)	Ni (w/o)	Cu (w/o)	Ni (w/o)	Cu (w/o)	Cr as FeCr (w/o)	Mn as FeMn (w/o)	P as Fe$_3$P (w/o)	Graphite (w/o)
A	--	--	--	--	--	--	--	0.45	--
B	0.85	--	--	1.0	--	0.9	0.75	--	0.4
C	--	--	--	2.0	--	--	--	--	0.6
D	--	--	--	--	2.0	--	--	--	0.9
E*	0.55	4.0	1.5	--	--	--	--	--	0.5
F	0.85	--	--	--	--	--	--	--	0.5
G*	0.55	2.0	1.5	--	--	--	--	--	0.5
H	1.50	--	--	2.0	--	--	--	--	0.4
I	0.85	--	--	2.0	--	--	--	--	0.5
J	0.85	--	--	--	--	--	1.0	--	0.4

*Diffusion Alloyed Base Material

Table II: Sintering and Heat Treatment Schedules by Density for the Tested Materials

Material	Density of Samples for Tests (g/cm³)			
	2050°F/1120°C As-Sintered	2300°F/1260°C As-Sintered	2050°F/1120°C Heat Treated	2350°F/1290°C Heat Treated
A	7.23, 7.40	7.33, 7.50	--	--
B	--	7.16*, 7.27*	--	7.16, 7.28
C	--	--	7.23	--
D	7.07, 7.17		--	--
E	7.19, 7.32	7.26, 7.37	7.20, 7.32	--
F	--	--	7.17, 7.30	--
G	--	--	7.19, 7.29	--
H	7.18, 7.34	7.21, 7.31	--	--
I	7.31	7.35	--	--
J	--	7.20*	--	--

*Sintered at 2350°F/1290°C

3.000"
+ 0.000"
- 0.004"

1.0"
±0.005"

1.000"
±0.010"

0.375" Dia.
+ 0.001"
- 0.000"

R = 1.3768"
±0.010"

0.1875" Dia.
±0.005"
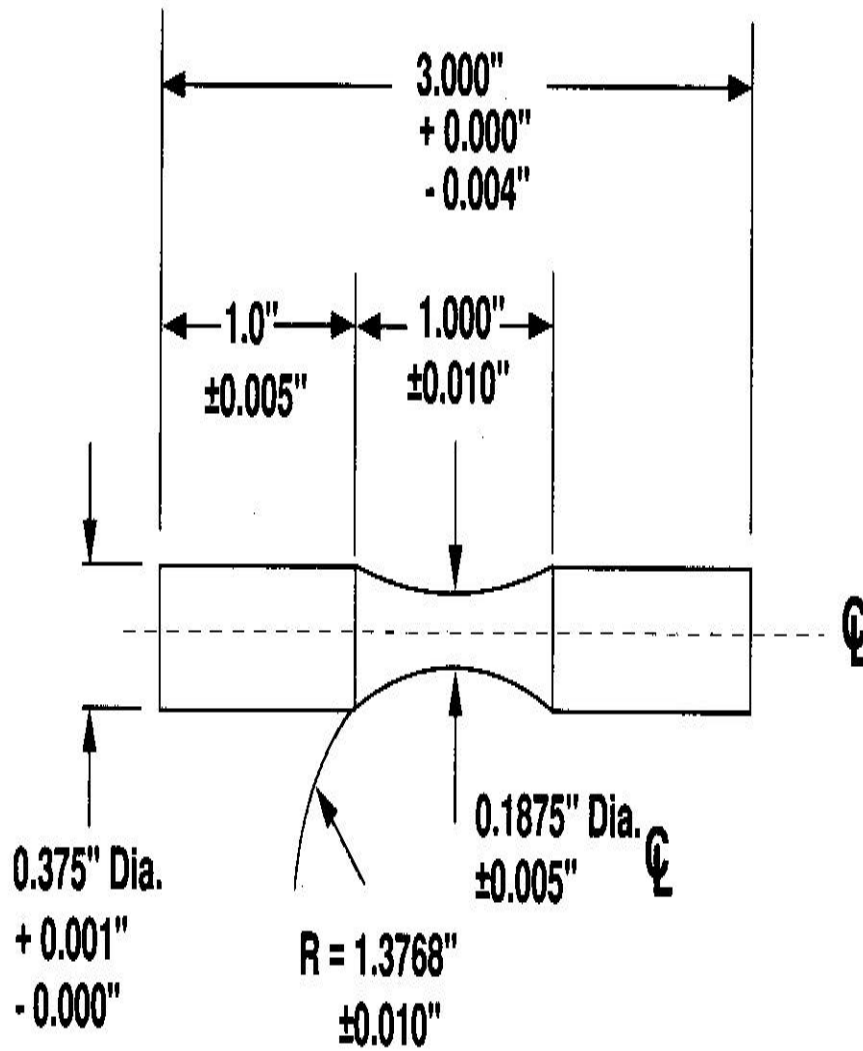
ALL DIAMETERS TO BE CONCENTRIC WITHIN 0.001"

SURFACE FINISH = 8 RMS (Polished Longitudinal)

Table III: Fatigue and Tensile Results for As-Sintered Materials Sintered at 2050°F/1120°C

Material	Sintering Temperature (°F/°C)	Heat Treat	Density (g/cm³)	50% FEL (10³psi / MPa)	99.9% FEL (10³psi/MPa)	Ultimate Tensile Strength (10³psi/MPa)
A	2050 / 1120	no	7.23	30.0 / 207	26.8 /185	53 / 365
			7.40	32.7 / 225	28.6 / 197	58 / 403
D	2050 / 1120	no	7.07	33.9 / 234	25.4 / 175	86 / 596
			7.17	35.3 / 243	28.0 / 193	90 / 621
E	2050 / 1120	no	7.19	33.3 / 230	26.3 / 181	103 / 710
			7.32	35.1 / 242	27.8 / 192	115 / 798
H	2050 / 1120	no	7.18	33.8 / 233	27.4 / 189	93 / 641
			7.34	38.0 / 262	35.0 / 241	101 / 693
I	2050 / 1120	no	7.31	36.7 / 253	32.2 / 222	91 / 632

Table IV: Fatigue and Tensile Results for As-Sintered Materials Sintered at 2300°F/1260°C (Materials B and J--2350°F/1290°C)

Material	Sintering Temperature (°F/°C)	Heat Treat	Density (g/cm³)	50% FEL (10³psi / MPa)	99.9% FEL (10³psi/MPa)	Ultimate Tensile Strength (10³psi/MPa)
A	2300 / 1260	no	7.33	31.4 / 216	29.7 / 205	59 / 403
			7.50	37.7 / 260	34.0 / 234	69 / 476
B	2350 / 1290	no	7.16	35.1 / 242	30.4 / 210	124 / 856
			7.27	39.2 / 270	34.0 / 234	133 / 917
E	2300 / 1260	no	7.26	31.5 / 217	24.9 / 172	118 / 814
			7.37	32.9 / 227	26.9 / 185	134 / 925
H	2300 / 1260	no	7.21	30.0 / 207	24.0 / 165	95 / 652
			7.37	37.1 / 256	29.2 / 201	103 / 710
I	2300 / 1260	no	7.35	35.8 / 247	31.7 / 219	98 / 672
J	2350 / 1290	no	7.20	34.6 / 239	32.9 / 227	90 / 621

Table V: Fatigue and Tensile Results for Heat Treated Materials Sintered at 2050°F/1120°C (Material B--2350°F/1290°C)

Material	Sintering Temperature (°F/°C)	Heat Treat	Density (g/cm³)	50% FEL (10³psi / MPa)	99.9% FEL (10³psi/MPa)	Ultimate Tensile Strength (10³psi/MPa)
B	2350 / 1290	yes	7.16	58.5 / 403	51.2 / 353	176 / 1211
			7.28	65.1 / 449	59.4 / 410	196 / 1349
C	2050 / 1120	yes	7.23	45.8 / 316	40.1 / 276	173 / 1193
E	2050 / 1120	yes	7.20	57.9 / 399	46.0 / 317	181 / 1249
			7.32	59.3 / 409	48.1 / 332	193 / 1327
F	2050 / 1120	yes	7.17	47.9 / 330	41.1 / 283	164 / 1131
			7.30	48.8 / 336	40.4 / 279	167 / 1151
G	2050 / 1120	yes	7.19	53.4 / 368	45.7 / 315	173 / 1192
			7.29	54.2 / 374	45.9 / 316	189 / 1303

Table VI: Microstructural Constituents for As-Sintered Materials Sintered at 2050°F/1120°C

Material	Sintering Temperature (°F/°C)	Heat Treat	Microstructure Constituents
A	2050 / 1120	no	Ferrite
D	2050 / 1120	no	Lamellar Pearlite, Light Ferrite, Dark Ferrite with Copper
E	2050 / 1120	no	Various Pearlite, Ni Rich Areas, Ferrite, Carbide Precipitates in Ferrite
H	2050 / 1120	no	Divorced Pearlite, Ni Rich Areas, Martensite, Unresolved Pearlite
I	2050 / 1120	no	Divorced Pearlite, Ni Rich Areas, Unresolved Pearlite

Table VII: Microstructural Constituents for As-Sintered Materials Sintered at 2300°F/1260°C (Materials B and J--2350°F/1290°C)

Material	Sintering Temperature (°F/°C)	Heat Treat	Microstructure Constituents
A	2300 / 1260	no	Ferrite, (larger grains than 2050°F/1120°C
B	2350 / 1290	no	Divorced Pearlite, Bainite, Alloy Rich Martensite
E	2300 / 1260	no	Divorced Pearlite, Unresolved Pearlite, Ni rich areas, Ferrite (larger grains and less Ni rich areas than 2050°F/1120°C)
H	2300 / 1260	no	Divorced Pearlite, Martensite (larger grains than 2050°F/1120°C)
I	2300 / 1260	no	Divorced Pearlite, Unresolved Pearlite, Ni rich areas (larger grains and less Ni rich areas than 2050°F/1120°C)
J	2350 / 1290	no	Divorced Pearlite

Table VIII: Microstructural Constituents for Heat Treated Materials Sintered at 2050°F/1120°C (Material B--2350°F/1290°C)

Material	Sintering Temperature (°C/°F)	Heat Treat	Microstructure Constituents
B	2350 / 1290	yes	Light and Dark Etching Martensite
C	2050 / 1120	yes	Martensite, Ni Rich Areas, Nodular Pearlite
E	2050 / 1120	yes	Martensite, Ni Rich Areas
F	2050 / 1120	yes	Martensite
G	2050 / 1120	yes	Martensite, Ni Rich Areas

Table IX: Stereological Data for As-Sintered Materials Sintered at 2050°F/1120°C

Material	Sintering Temperature (°F/°C)	Heat Treat	Density (g/cm³)	Mean Pore Spacing (µm)	Mean Pore Size (µm)	Number of Pores per 1000 µm²
A	2050 / 1120	no	7.23	77	50	142
			7.40	85	33	161
D	2050 / 1120	no	7.07	61	45	145
			7.17	68	31	170
E	2050 / 1120	no	7.19	58	38	205
			7.32	70	27	201
H	2050 / 1120	no	7.18	62	40	191
			7.34	74	34	168
I	2050 / 1120	no	7.31	74	27	195

Table X: Stereological Data for As-Sintered Materials Sintered at 2300°F/1260°C
(Materials B and J--2350°F/1290°C)

Material	Sintering Temperature (°F/°C)	Heat Treat	Density (g/cm³)	Mean Pore Spacing (µm)	Mean Pore Size (µm)	Number of Pores per 1000 µm²
A	2300 / 1260	no	7.33	112	73	85
			7.50	172	52	72
B	2350 / 1290	no	7.16	72	64	110
			7.27	88	46	132
E	2300 / 1260	no	7.26	70	34	194
			7.37	75	27	195
H	2300 / 1260	no	7.21	64	51	159
			7.37	87	32	165
I	2300 / 1260	no	7.35	83	39	147
J	2350 / 1290	no	7.20	35	50	138

Table XI: Stereological Data for Heat Treated Materials Sintered at 2050°F/1120°C
(Material B--2350°F/1290°C)

| Material	Sintering Temperature (°F/°C)	Heat Treat	Density (g/cm³)	Mean Pore Spacing (µm)	Mean Pore Size (µm)	Number of Pores per 1000 µm²
B	2350 / 1290	yes	7.16	74	65	116
			7.28	84	44	135
C	2050 / 1120	yes	7.23	59	31	221
E	2050 / 1120	yes	7.20	62	31	215
			7.32	72	25	212
F	2050 / 1120	yes	7.17	63	45	180
			7.30	72	32	176
G	2050 / 1120	yes	7.19	62	36	198
			7.29	64	31	194

6
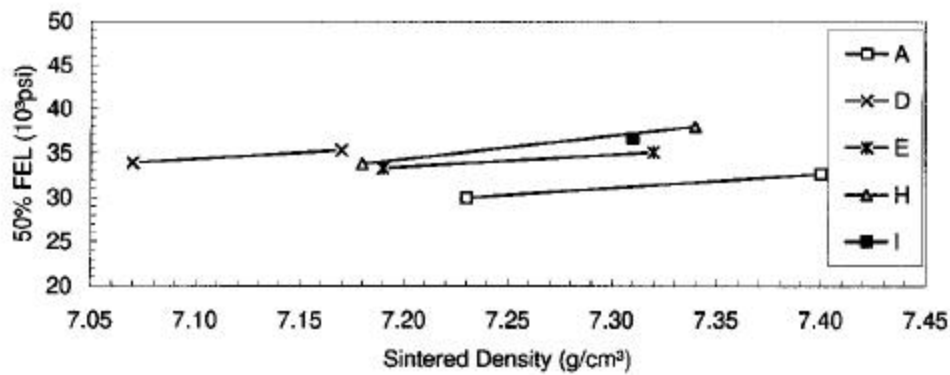
Figure 2: The Effect of Density on Fatigue Properties of As-Sintered (2050°F/1120°C) Materials
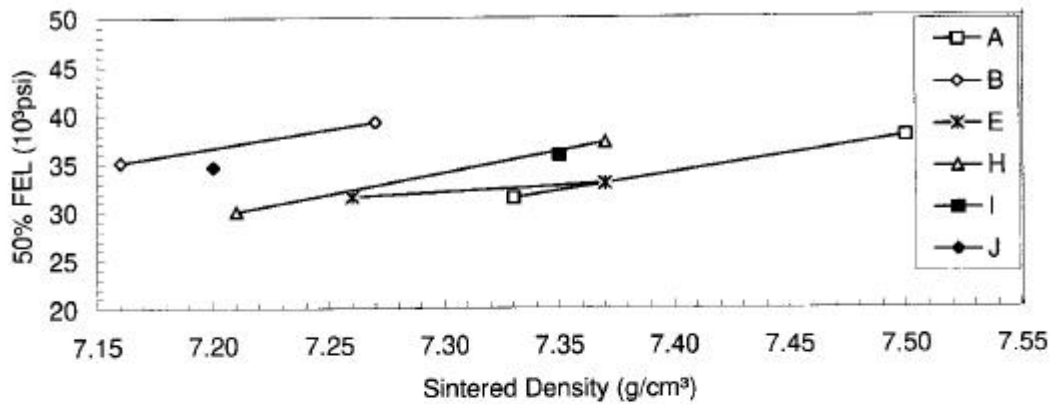

Figure 3: The Effect of Density on Fatigue Properties of As-Sintered (2300°F/1260°C, B and J--2350°F/1290°C) Materials
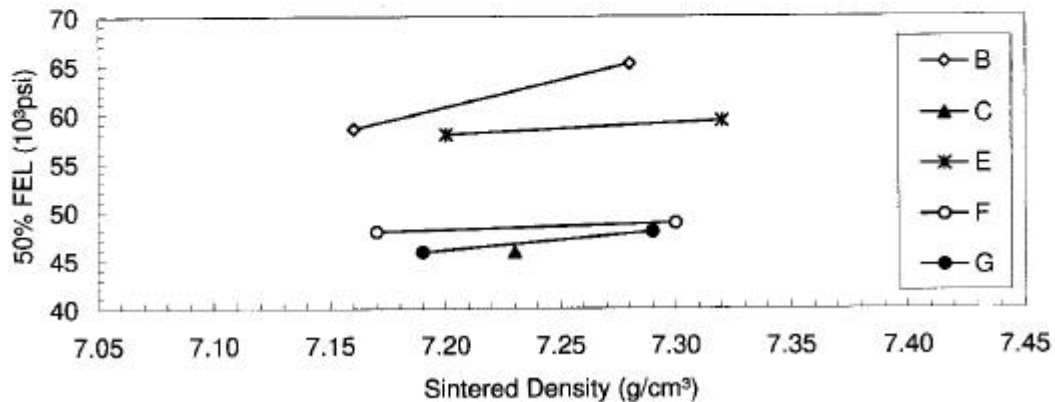

Figure 4: The Effect of Density on Fatigue Properties of Heat Treated (2050°F/1120°C except B--2350°F/1290°C) Materials
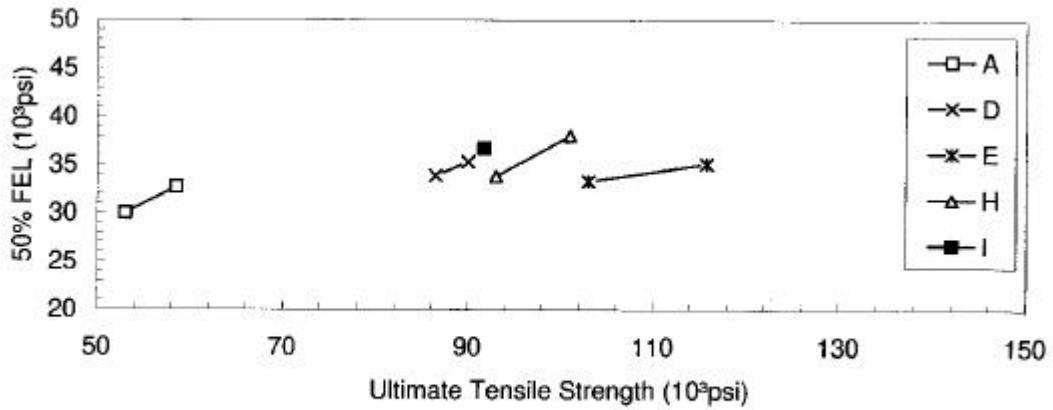
**Figure 5: The Effect of Ultimate Tensile Strength on Fatigue Properties of As-Sintered (2050°F/1120°C) Materials**
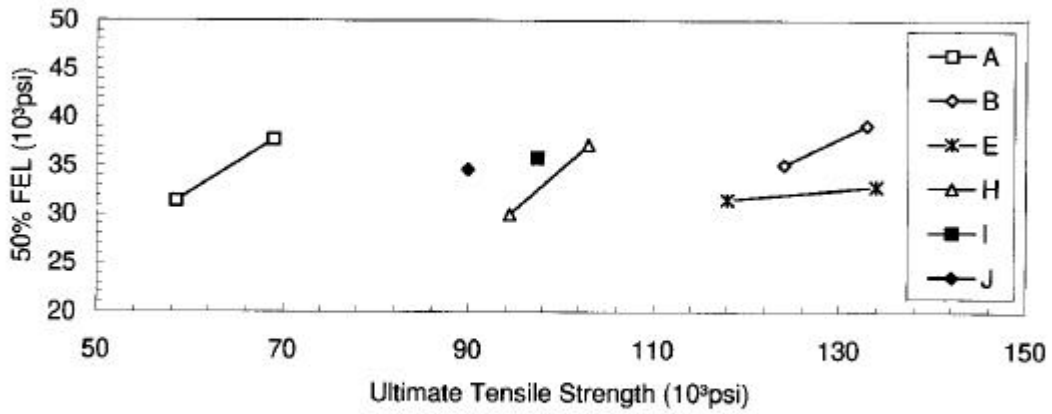
Figure 6: The Effect of Ultimate Tensile Strength on Fatigue Properties of As-Sintered (2300°F/1260°C, B and J--2350°F/1290°C) Materials
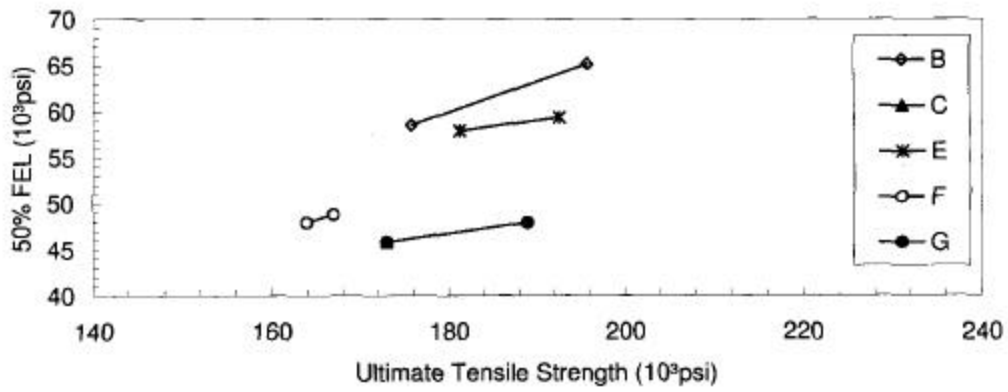
Figure 7: The Effect of Ultimate Tensile Strength on Fatigue Properties of Heat Treated (2050°F/1120°C except B--2350°F/1290°C) Materials
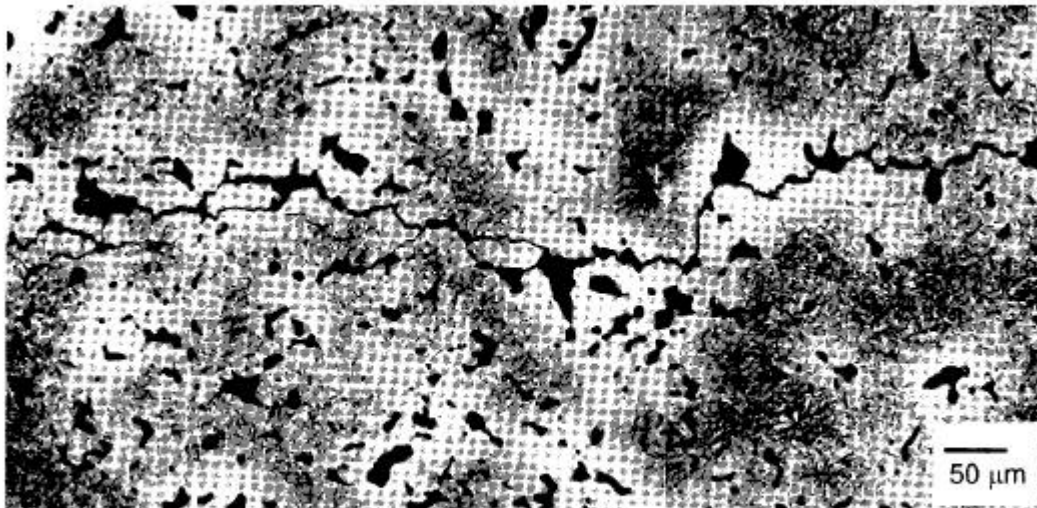
Figure 8: The Heat Treated Microstructure of Material B showing Crack Propagation in the Light Etching Areas (Etched--2% Nital, Original Magnification--200X)

16

2050°F/1120°C   2300°F/1260°C
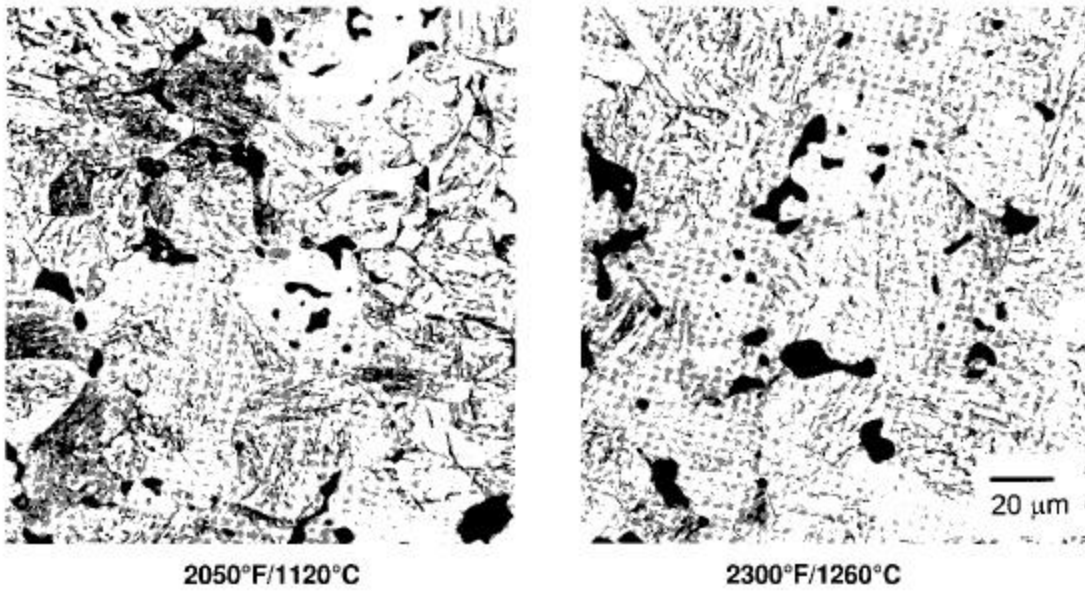
Figure 9:   The Effect of Sintering Temperature on Grain Size For Material I (Etch--2% Nital, Original Magnification--500X)
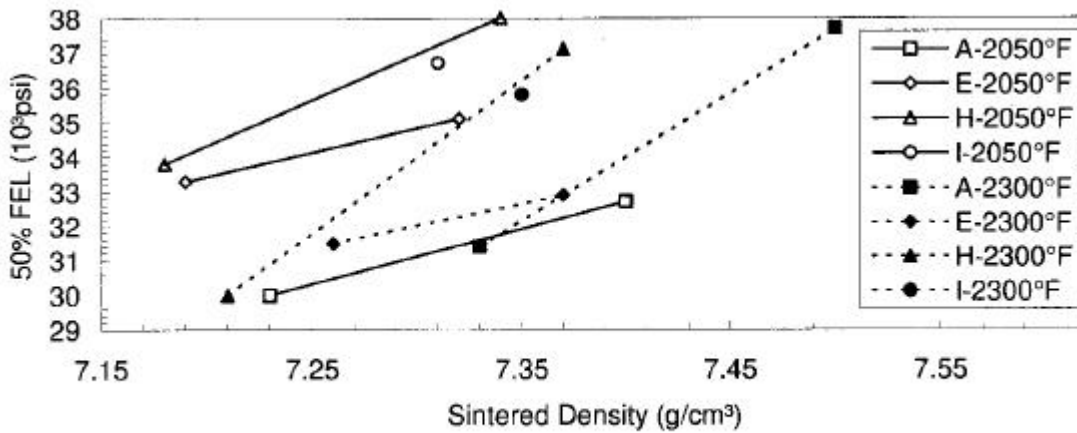

Figure 10: The Effect of Sintering Temperature and Density on Fatigue Properties

17
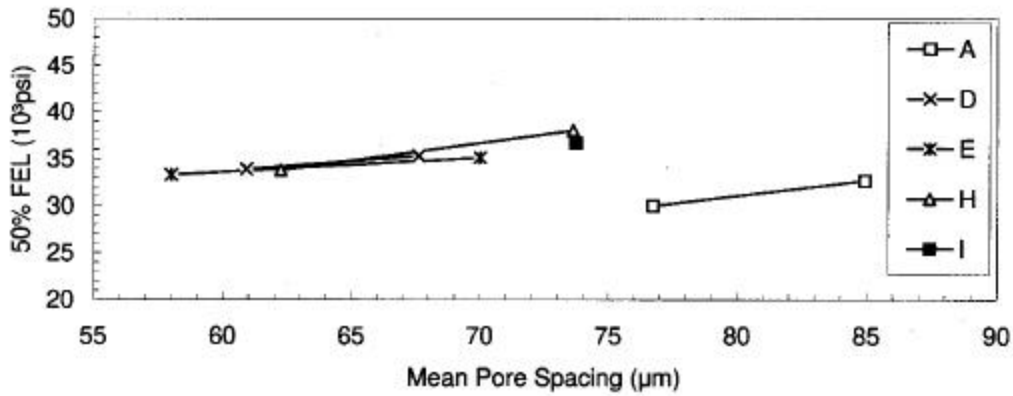
Figure 11: The Effect of Mean Pore Spacing on Fatigue Properties of As-Sintered (2050°F/1120°C) Materials
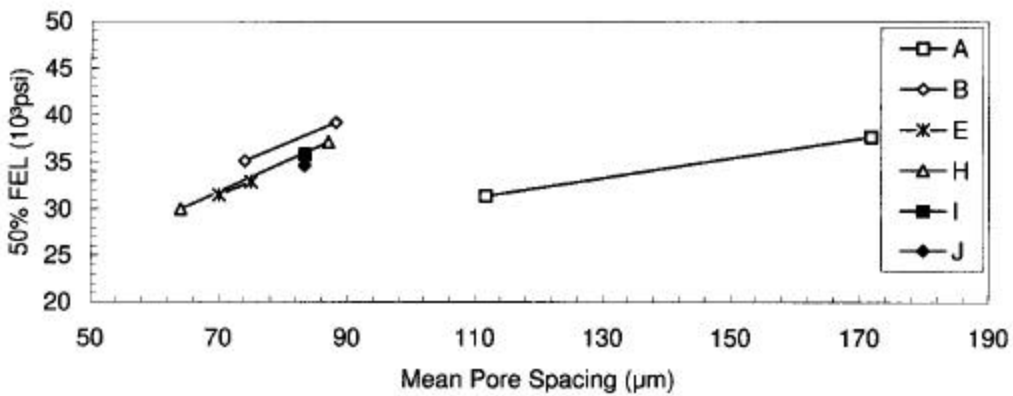

Figure 12: The Effect of Mean Pore Spacing on Fatigue Properties of As-Sintered (2300°F/1260°C except B and J--2350°F/1290°C) Materials
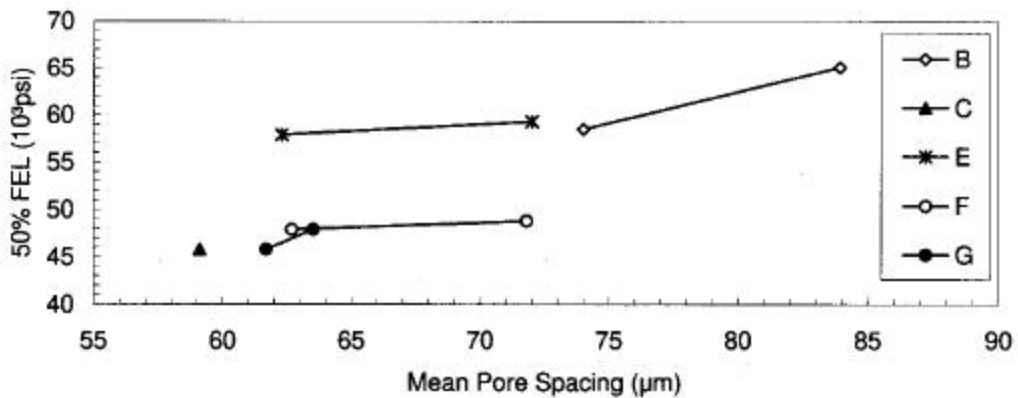

Figure 13: The Effect of Mean Pore Spacing on Fatigue Properties of Heat Treated Materials
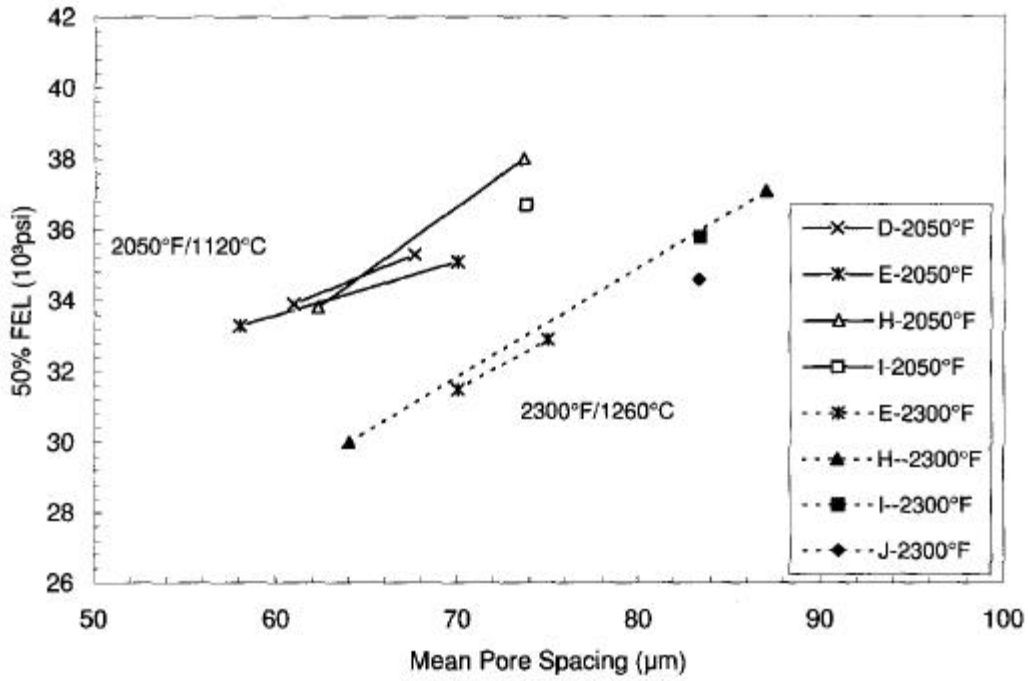
Figure 14: A Comparison of Mean Pore Spacing and 50% FEL Relationships for Four Materials Sintered at Two Temperatures